NiSi crystal structure, site preference, and partitioning behavior of palladium in NiSi(Pd)/Si(100) thin films: Experiments and calculations

Zugang Mao,[1,a)] Yeong-Cheol Kim,[2,b)] Hi-Deok Lee,[3,c)] Praneet Adusumilli,[1,d)] and David N. Seidman[1,e)]
[1]*Department of Materials Science and Engineering, Northwestern University, 2220 Campus Drive, Evanston, Illinois, 60208-3108*
[2]*School of Materials, and Chemical Engineering, Korea University of Technology and Education, Cheonan, 330-708, Korea*
[3]*Department of Electronics Engineering, Chungnam National University, Daejeon, 305-764, Korea*

(Received 11 April 2011; accepted 6 June 2011; published online 6 July 2011)

The crystal structure of a NiSi thin-film on a Si substrate and Pd site-substitution in NiSi and the partitioning behavior of Pd for NiSi(Pd)/Si(100) are investigated by x-ray diffraction (XRD), first-principles calculations, and atom-probe tomography (APT). The NiSi layer is a distorted orthorhombic structure from XRD patterns via experiments and calculations. We find that Pd has a strong driving force, 0.72 eV atom^{-1}, for partitioning from Si into the orthorhombic NiSi layer. The calculated substitutional energies of Pd in NiSi indicate that Pd has a strong preference for Ni sublattice-sites, which is in agreement with concentration profiles determined by APT. © *2011 American Institute of Physics*. [doi:10.1063/1.3606536]

Transition-metal silicide thin-films are extensively studied and widely used due to their low-resistivity in micro- and nano-electronic devices.[1–6] NiSi has been used for contact applications in the source, drain, and gate regions of complementary metal-oxide-semiconductor (CMOS) field-effect transistors, since 65 nm technology node. Fully silicided (FUSI) NiSi gates manufactured by a two-step self-aligned (salicide) process are also being actively studied.[7] Though NiSi has been researched since the 1970s, it assumes renewed significance due to its imminent implementation in high-dielectric constant (κ) and metal-gate technology for the 45 nm technology node onwards.[8] NiSi has a lower temperature of formation, lower resistivity in narrow dimensions, and lower Si consumption, making it preferable to $TiSi_2$ and $CoSi_2$ contacts.[7,9] To better understand the electronic properties of NiSi, it is very important to study the formation mechanism and crystal structure of NiSi. Since NiSi's formation kinetics is controlled by diffusion of nickel,[10] it leads to smoother interfaces. The thermal stability of NiSi is, however, a major challenge that needs addressing for its successful implementation. At elevated temperatures, NiSi degrades via two mechanisms: (a) agglomeration of the NiSi phase and (b) phase transformation to the higher resistivity $NiSi_2$ phase, both of which cause an increase in resistivity.[10] The addition of transition elements, Pd, Pt, Co, stabilizes NiSi and increases the thermal window for processing.[7,11–13] In this article, we present a study of the Ni-Pd-Si system to understand the mechanism of NiSi's stabilization, experimentally and theoretically. We performed both structural characterization and atom-probe tomography (APT) at the sub-nanoscale and first-principles calculations to gain atomistic insights.

[a)]Electronic mail: z-mao2@northwestern.edu.
[b)]Electronic mail: yckim@kut.ac.kr.
[c)]Electronic mail: hdlee@cnu.ac.kr.
[d)]Electronic mail: praneet@northwestern.edu.
[e)]Author to whom correspondence should be addressed. Electronic mail: d-seidman@northwestern.edu.

Laser-assisted local-electrode atom-probe (LEAP) tomography utilized a pulsed laser to dissect specimens on an atom-by-atom basis at 40 K under ultrahigh vacuum conditions ($<10^{-10}$ Torr). A pulsed picosecond laser (wavelength = 532 nm) operating at 250 kHz, 0.5 nJ pulse^{-1}, was employed to dissect a specimen with a 10 nm Ni(Pd) layer and a micro-tip length of 500 nm. LEAP tomographic samples were fabricated using a FEI Nova dual-beam focused ion-beam (FIB) microscope employing the lift-out technique.[14,15]

Ni-Pd-Si samples were prepared as follows. Specifically, $Ni_{1-x}Pd_x$(x = 5 at. %) films were deposited by radio-frequency magnetron sputtering on p-type Si(100) substrates after removing the native oxide employing a 2% buffered HF solution. Using sheet resistance measurements as an indicator of the formation and persistence of the NiSi phase, it was determined that $Ni_{0.95}Pd_{0.05}$ had the broadest thermal processing window among three concentrations, 1, 5, 10 at.%, Fig. 1. Hence, the $Ni_{0.95}Pd_{0.05}$/Si(100) sample subjected to rapid thermal annealing (RTP) at 600 °C was selected; it was then annealed at 650 °C for 30 min in N_2 at an ambient pressure of one atom to approximate the effects of subsequent thermal treatments experienced by silicide contacts during the CMOS fabrication process. High resolution field-emission scanning electron microscopy (HRSEM) imaging (not displayed) demonstrated that $Ni_{0.95}Pd_{0.05}$ showed uniform interface with Si even after 650 °C annealing for 30 min, and high resolution grazing incidence x-ray diffraction (XRD) confirmed that nickel monosilicide (NiSi) was the only silicide phase present; diffraction peaks corresponding to $NiSi_2$ or PdSi were not detected.

The electronic structures of pure NiSi and the sublattice site-preference of the dopant, Pd, were studied using first-principles calculations: full-electron (WIEN2K) (Ref. 16) and pseudo-potential calculations (VASP) (Refs. 17, 18) were utilized. Full-electron self-consistent calculations of the electronic structure and optical properties based on the scalar relativistic full-potential linearized augmented plane-wave

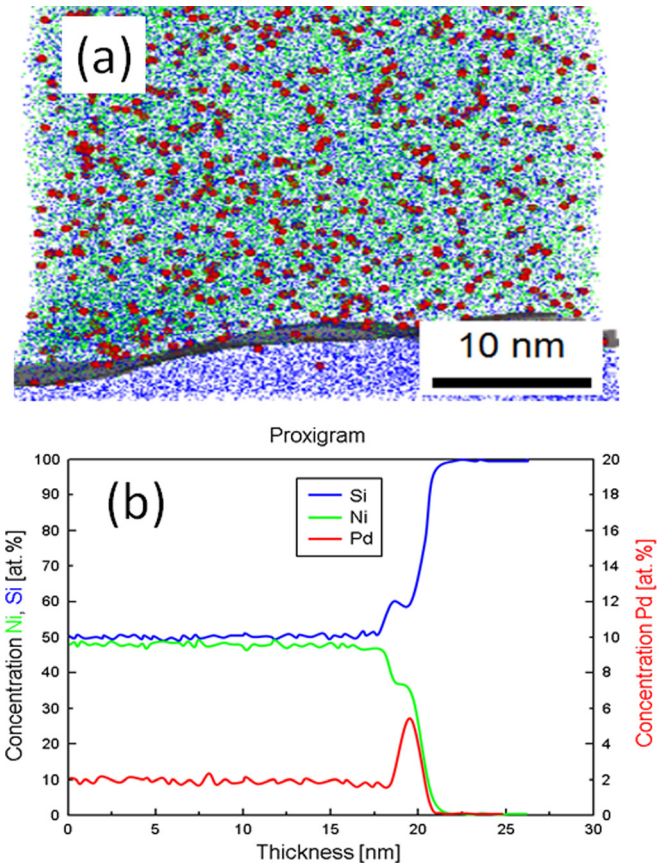

FIG. 1. (Color online) (a) Two-dimensional projection of the full three-dimensional reconstruction of LEAP tomography data showing the distribution of elements and the isoconcentration surface (shaded sheet) that defines the heterophase interface. (b) Proximity histogram displaying the concentrations of Ni, Si, and Pd versus film-depth. Concentrations were calculated for a series of isoconcentration surfaces moving into the thin film.

method (FP-LAPW) were performed using the WIEN2K package. These calculations were used to determine the preferred NiSi crystal structure and benchmark the accuracy of the pseudo-potentials. To achieve energy convergence, the wave functions in the interstices were expanded in plane waves with a cut-off $K_{\max} = 9/R_{\mathrm{MT}}$. The self-consistent calculations were assumed to be converged when the total energy of the system was stable to 10^{-5} Ry. Pseudo-potential (PP) calculations were performed to determine the site preference of Pd, with the projected augmented wave[19] (PAW) method with the LDA method, as implemented in VASP. We employed spin-polarized (ferromagnetic) calculations and an optimized energy cutoff of 300 eV was utilized with 0.121 Å^{-1} spacing Monkhorst-Pack **k**-point grids. The energy per unit cell converged to 2×10^{-5} eV atom^{-1} and the residual forces to 0.005 eV nm^{-1}.

The physical properties of NiSi have yet to be fully studied both experimentally and theoretically. NiSi has two possible crystal structures: cubic (B2) (Ref. 20) and orthorhombic. The orthorhombic structure of bulk NiSi is pseudo-hexagonal and conceptually is a distorted NiAs structure.[21] Both Ni and Si occupy position 4c (site symmetry m) with atomic positional parameters (x, 0.25, z) and (x, 0.75, z), respectively. The NiSi orthorhombic structure was determined by experimental XRD studies at 295 K.[22,23] It is needed to determine which structure, B2 or orthorhombic, is formed in NiSi thin-films on a Si substrate.

In this article, two possible crystal structures of NiSi, B2 and orthorhombic, are fully relaxed by FP-LAPW, Table I. From our calculations, the orthorhombic structure has a more negative formation energy (−0.891 eV·atom^{-1}) than the B2 structure (−0.797 eV atom^{-1}). Energetically, the orthorhombic structure is preferred and the B2 structure is metastable with respect to it. The simulated lattice parameters of an orthorhombic unit cell are in excellent agreement with experimental reports.[22,23]

The simulated x-ray diffraction patterns for the fully relaxed orthorhombic and B2 structures are displayed in Figures 2(b) and 2(c). There are only three distinguishable peaks at 31.5° (001), 44.8° (011), and 65.5° (002) for the B2 structure for 2θ between 20° and 80°. The diffraction spectra for the orthorhombic structure are completely different, especially the distinct peaks between 45 and 60°; there is no peak for B2 in the same 2θ region. The experimental XRD spectrum shows no significant peaks in the same 2θ range as the B2 structure. All significant peaks in the experimental XRD spectra are close to the calculated orthorhombic pattern, especially those peaks between 45 and 60°. Thus, we conclude that the crystal structure of a NiSi thin-film is close to a distorted orthorhombic structure, Figure 2. This result is in agreement with the orthorhombic structure having more negative formation energy than the metastable B2 structure from FP-LAPW calculations.

The same calculations were performed by using PPs, which are in reasonable agreement with the FP-LAPW calculations, Table I. Both potentials demonstrate that the orthorhombic structure has the smaller formation energy. PP calculations can provide reliable insights into the substitutional-site preference in the orthorhombic structure and the partitioning behavior of Pd between NiSi and Si.

The compositional proxigram determined using APT yields 48.09Ni-1.99Pd-49.92Si (at. %), Figure 1, in the NiSi layer, suggesting strongly that Pd prefers Ni sublattice sites to form $(Ni_{1-x}Pd_x)Si$. We also found that Pd partitions strongly to the NiSi layer: the concentration of Pd in Si is 0.1 at. %. PP methods were used to calculate the site preference for Pd in an orthorhombic superlattice: $2 \times 2 \times 2$ unit cells containing 64 atoms were employed. The substitutional preference is determined from the substitutional energies, $E_{Pd \to Ni}$ and $E_{Pd \to Si}$, which are defined as

$$E_{Pd \to Ni} = [(E^{TOT}_{(Ni_{1-x}Pd_x)Si} + n_{Ni}\mu_{Ni}) - (E^{TOT}_{NiSi} + n_{Pd}\mu_{Pd})]/n, \quad (1)$$

TABLE I. Comparison of the lattice parameters and the crystal formation energies of orthorhombic and NiSi(B2) crystal structures from FP-LAPW and PP calculations.

	Orthorhombic		B2	
	FP-LAPW	PP	FP-LAPW	PP
Lattice parameter (Å)	$a = 5.285$ $b = 3.282$ $c = 4.505$	$a = 5.191$ $b = 3.234$ $c = 4.483$	2.835	2.825
Formation energy (eV·atom^{-1})	−0.891	−0.636	−0.797	−0.539

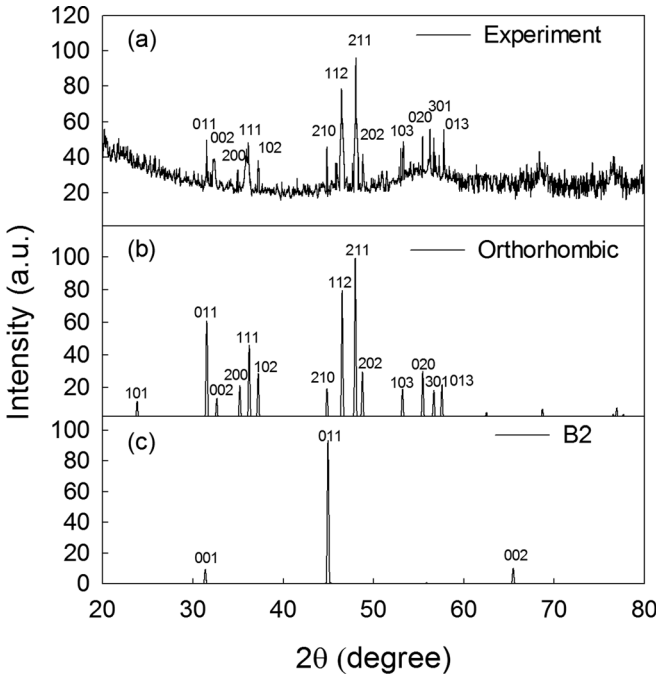

FIG. 2. X-ray diffraction spectra of NiSi: (a) experimentally determined; (b) calculated NiSi orthorhombic structure; and (c) calculated NiSi(B2) structure.

$$E_{Pd\rightarrow Al} = [(E^{TOT}_{Ni(Al_{1-y}Pd_y)} + n_{Si}\mu_{Si}) - (E^{TOT}_{NiSi} + n_{Pd}\mu_{Pd})]/n, \quad (2)$$

where n is the number of atoms and μ is a chemical potential, which are determined from their elemental bulk energy per atom in the same cell symmetry, Table II. These first-principles results demonstrate that Pd prefers strongly Ni sublattice sites over Si sublattice sites. Kinetically, Pd atoms diffuse between Si(Pd) and $(Ni_{1-x}Pd_x)Si$ because of a chemical potential gradient between them. The calculated energy difference for Pd between Si(Pd) and the $(Ni_{1-x}Pd_x)Si$ layer is 0.7191 eV atom^{-1}, which results in Pd partitioning to the $(Ni_{1-x}Pd_x)Si$ layer. This result is in excellent agreement with experimental results for a small Pd concentration in Si.[15]

The average atomic displacements and forces associated with the local strains and stresses resulting from substitution of Pd on the Ni and Si sublattice sites in NiSi and in Ni(f.c.c.) are listed in Table II. Both the average atomic displacements and forces from substitution in Ni sublattice sites of NiSi are found to be significantly smaller than for substitution in Si sublattice sites. We also find the average atomic displacements and forces for substitutions in pure Si (or Ni) to be larger than those for substitution in NiSi.

In summary, the crystal structure of NiSi, site substitution, and partitioning behavior of Pd in NiSi/Si(100) thin-films are investigated by APT and first-principles calculations. The NiSi layer is determined to be a distorted orthorhombic structure from XRD experiments and theoretical calculations. The calculated substitutional energies of Pd atoms at Ni and Si sublattice sites indicate that Pd has a strong preference for Ni sublattice sites and has a strong driving force to partition to the NiSi layer from Si, which are in agreement with experimentally determined APT concentration profiles. Experimentally, the Pd concentration in Si is 0.1 at. %.

TABLE II. Substitutional energy, average atomic force, and displacement at the first nearest-neighbor distance of Pd in orthorhombic NiSi, Ni(f.c.c.) and diamond-cubic Si were calculated using the DFT LDA method from first-principles calculations.

	E_{sub}(eV atom^{-1})	Average atomic force (eV Å^{-1})	Average atomic displacement (Å)
$(Ni_{1-x}Pd_x)Si$	−0.2619	0.0274	0.095
$Ni(Si_{1-x}Pd_x)$	1.4310	0.0396	0.204
$Ni_{1-x}Pd_x$	0.3436	0.0314	0.110
$Si_{1-x}Pd_x$	0.4572	0.0421	0.332

P.A. thanks IBM for a fellowship and the US-Israel Binational Foundation for partial support. This study was supported by the Semiconductor Research Corporation through Task No. 1441.001 and the Korea Science and Engineering Foundation (KOSFET) through the Basic Science Programs for General Research Grant (No. 2009-0076318). APT measurements were performed in the Northwestern University Center for Atom-Probe Tomography (NUCAPT).

[1]R. Pretorius, C. L. Ramiller, S. S. Lau, and M. A. Nicolet, Appl. Phys. Lett. **30**(10), 501 (1977).
[2]S. Petersson, E. Mgbenu, and P. A. Tove, Phys. Status Solidi A **36**(1), 217 (1976).
[3]J. O. Olowolafe, K. Nakamura, S. S. Lau, M. A. Nicolet, J. W. Mayer, and R. Shima, J. Appl. Phys. **47**, 1278 (1976).
[4]J. M. Poate, W. L. Brown, R. Homer, W. M. Augustyniak, J. W. Mayer, K. N. Tu, and W. F. Vanderweg, Nucl. Instrum. Methods **132**(Jan-F), 345 (1976).
[5]E. I. Alessandrini, D. R. Campbell, and K. N. Tu, J. Vac. Sci. Technol. **13**(1), 55 (1976).
[6]J. Baglin, R. Anderson, J. Dempsey, W. Hammer, F. d'Heurle, and S. Petersson, Appl. Phys. Lett. **35**, 285 (1979).
[7]T. Morimoto, T. Ohguro, H. S. Momose, T. Iinuma, I. Kunishima, K. Suguro, I. Katakabe, H. Nakajima, M. Tsuchiaki, M. Ono, Y. Katsumata, and H. Iwai, IEEE Trans. Electron Devices **42**(5), 915 (1995).
[8]Y. Mishima, S. Ochiai, and T. Suzuki, Acta Metall. **33**(6), 1161 (1985).
[9]E. G. Moroni, R. Podloucky, and J. Hafner, Phys. Rev. Lett. **81**(9), 1969 (1998).
[10]C. Detavernier, C. Lavoie, C. Cabral, Jr., F. M. d'Heurle, A. J. Kellock, J. Jordan-Sweet, and J. M. E. Harper, Microelectron. Eng. **83**, 2042 (2006).
[11]F. M. d'Heurle, J. Electron. Mater. **27**, 1138 (1998).
[12]S. L. Zhang, Microelectron. Eng. **70**, 174 (2003).
[13]C. Detavernier, C. Lavoie, and P. Besser, *Nickel Silicide Technology*, edited by L. J. Chen, C. Lavoie, C. Detavernier, and P. Besser (IEE, London, 2004).
[14]Y. C. Kim, P. Adusumilli, L. J. Lauhon, D. N. Seidman, S. Y. Jung, H. D. Lee, R. L. Alvis, R. M. Ulfig, and J. D. Olson, Appl. Phys. Lett. **91**(11), (2007).
[15]K. Thompson, D. Lawrence, D. J. Larson, J. D. Olson, T. F. Kelly, and B. Gorman, Ultramicroscopy **107**(2–3), 131 (2007).
[16]P. Blaha, K. Schwarz, P. Sorantin, and S. B. Trickey, Comput. Phys. Commun. **59**(2), 399 (1990).
[17]G. Kresse, J. Non-Cryst. Solids **205–207**(Pt. 2), 833 (1996).
[18]G. Kresse and J. Furthmueller, Phys. Rev. B: Condens. Matter **54**(16), 11169 (1996).
[19]G. Kresse and D. Joubert, Phys. Rev. B **59**(3), 1758 (1999).
[20]G. Profeta, S. Picozzi, A. Continenza, G. Schneider, and R. Podloucky, J. Magn. Magn. Mater. **272**, E233 (2004).
[21]E. I. Gladyshevskii, *Kristallokhimiya silitsidov i germanidov (Crystal Chemistry of Silicides and Germanides)* (Metallurgiya, Moscow, 1971).
[22]M. B. Ataev and M. Kh. Rabadanov, Inorg. Mater. **38**, 120 (2002).
[23]M. B. Ataev and M. Kh. Rabadanov, Crystallogr. Rep. **47**, 379 (2001).